Geophysical Research Letters

RESEARCH LETTER
10.1029/2019GL085649

Does a Damaged-Fault Zone Mitigate the Near-Field Impact of Supershear Earthquakes?—Application to the 2018 M_w 7.5 Palu, Indonesia, Earthquake

Elif Oral[1], Huihui Weng[1], and Jean Paul Ampuero[1,2]

[1]Université Côte d'Azur, IRD, CNRS, Observatoire de la Côte d'Azur, Géoazur, France, [2]Seismological Laboratory, California Institute of Technology, Pasadena, CA, USA

Key Points:
- The unexpected supershear but sub-Eshelby rupture speed of the 2018 Palu earthquake can be explained by a fault damage zone
- The reduction of rupture speed by a fault damage zone mitigates the near-field ground motion and landslide hazard
- Fault zone waves could have amplified ground motions, but not enough to compensate for the mitigation effect of reduced rupture speed

Supporting Information:
- Supporting Information S1

Correspondence to:
E. Oral,
elif.oral@geoazur.unice.fr

Citation:
Oral, E., Weng, H., & Ampuero, J. P. (2020). Does a damaged-fault zone mitigate the near-field impact of supershear earthquakes?—Application to the 2018 M_w 7.5 Palu, Indonesia, earthquake. *Geophysical Research Letters*, *47*, e2019GL085649. https://doi.org/10.1029/2019GL085649

Received 2 OCT 2019
Accepted 23 DEC 2019
Accepted article online 3 JAN 2020

Abstract The impact of earthquakes can be severely aggravated by cascading secondary hazards. The 2018 M_w 7.5 Palu, Indonesia, earthquake led to devastating tsunamis and landslides, while triggered submarine landslides possibly contributed substantially to generate the tsunami. The rupture was supershear over most of its length, but its speed was unexpectedly slow for a supershear event, between the S wave velocity V_S and Eshelby's speed $\sqrt{2}V_S$, an unstable speed range in conventional theory. Here, we investigate whether dynamic rupture models including a low-velocity fault zone can reproduce such a steady supershear rupture with a relatively low speed. We then examine numerically how this peculiar feature of the Palu earthquake could have affected the near-field ground motion and thus the secondary hazards. Our findings suggest that the presence of a low-velocity fault zone can explain the unexpected rupture speed and may have mitigated the near-field ground motion and the induced landslides in Palu.

Plain Language Summary Earthquakes are produced by slippage quickly unzipping along faults, causing Earth's vibrations, that is, ground shaking. The impact of the earthquake can become more catastrophic by triggered phenomena, like landslides and tsunamis, as witnessed during the 2018 Palu (Indonesia) earthquake of magnitude 7.5. Generally, the faster the earthquake rupture, the stronger the shaking. The Palu earthquake is among a class of very fast but rare earthquakes whose speed exceeds that of shearing waves in rocks. Theoretically, these so-called "supershear earthquakes" can propagate steadily only if faster than a speed known as Eshelby's speed. Surprisingly, the Palu earthquake is slower than this limit. How can we explain this unusual speed? Did it affect the triggering of landslides, including submarine landslides that likely contributed to the tsunami? We address these questions through computer simulations, particularly focusing on the possible effect of a "fault damage zone," a layer of softened rocks surrounding faults and caused by rock fracturing accumulated throughout the past fault activity. We found that, if a damage zone exists around the Palu fault, it can explain the unusual speed of this supershear earthquake and may have had the beneficial effect of reducing the shaking and thus its induced landslide and tsunami hazards in Palu.

1. Introduction

The 2018 M_w 7.5 earthquake in Palu (Sulawesi, Indonesia) ruptured at a supershear speed; that is, the rupture speed exceeded the shear wave speed of the medium. The rupture initiated on an unmapped fault located within the inland Sulawesi neck and propagated 150 km southward on the strike-slip Palu-Koro fault (Bao et al., 2019; Socquet et al., 2019) (Figure 1a). Studies using teleseismic backprojection revealed that the rupture rapidly reached a steady velocity of about $V_{rup} = 4.1$ km/s, exceeding the local S wave velocity $V_S = 3.4$–3.8 km/s (Bao et al., 2019).

The rupture of the Palu earthquake was faster than most earthquakes but slower than a usual supershear earthquake, and here we aim to understand whether the presence of a damaged-fault zone can be the reason behind it. On the basis of theoretical and experimental studies, a stable rupture propagation at supershear speed is only expected at velocities higher than Eshelby's speed $V_E = \sqrt{2}V_S$ (Andrews, 1976; Dunham, 2007). Yet the inferred rupture speed of the Palu event lies in the unstable supershear regime $V_S < V_{rup} < V_E$. One proposed explanation of such a rupture speed is the presence of a low-velocity fault zone (LVFZ). Supershear ruptures in a LVFZ approach the P wave speed of the LVFZ (Huang et al., 2016; Harris & Day, 1997). Indeed, Bao et al. (2019) interpreted the observed rupture speed by the possible presence of a LVFZ with

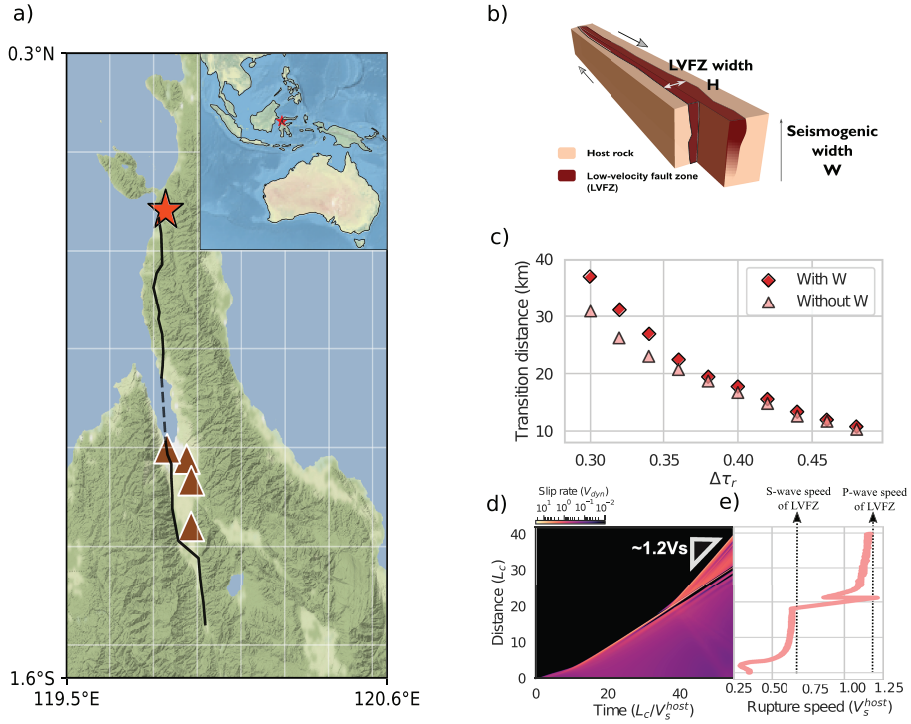

Figure 1. (a) Location map of the Palu earthquake epicenter (star), fault rupture trace (black line), and triggered landslides (triangles). (b) Conceptual model of a low-velocity fault zone. (c) Supershear transition distance as a function of stress drop (normalized by strength drop) in dynamic rupture models with and without finite seismogenic zone. (d) Spatiotemporal distribution of slip rate and (e) rupture speed versus distance along the fault strike for the simulation where $\Delta\tau_r = 0.37$.

30% velocity reduction. However, previous studies modeling supershear rupture in a LVFZ were based on 2-D models that ignored the finiteness of the seismogenic depth, while the Palu earthquake rupture has a high length-to-width ratio (150-km length vs. a typical seismogenic depth of 15–20 km for strike-slip earthquakes). Recent theory and simulations show that the seismogenic width controls the evolution of rupture speed in elongated faults (Weng & Ampuero, 2019). Thus, the first question we address, in section 2, is: Can the presence of a LVFZ lead to a steady-state supershear rupture running at the damaged-rock *P* wave speed in a long rupture with finite seismogenic width?

The earthquake also triggered devastating landslides; the rupture properties must also have been determinant on the distribution and density of coseismic landslides in addition to site and path effects, and other local aggravating conditions such as irrigation practice (Bradley et al., 2019; Watkinson & Hall, 2019). The impact of the earthquake was aggravated by landslides triggered in the proximity of the fault, including submarine landslides in the Palu Bay that likely contributed to the generation of a devastating tsunami (Carvajal et al., 2019). Major coseismic landslides were reported in four different areas, within 10 km of distance from the fault (Figure 1a), on gently sloping alluvial valley floor. Past studies have relied on the empirical evaluation of earthquake-induced landslide hazard by using seismic factors such as earthquake magnitude and epicentral distance (e.g., Keefer, 1984; Meunier et al., 2007; Papadopoulos & Plessa, 2000). Yet recent research points to the necessity of considering the combined effect of geo-environmental factors and rupture complexities to improve the hazard prediction. For example, landslides triggered by the 2008 Wenchuan, China, earthquake were found to be unexpectedly high for a M_w 7.9 event (Xu et al., 2016). Conversely, the 1999 M_w 7.2 Düzce, Turkey, and the 2002 M_w 7.9 Denali, USA, earthquakes induced fewer landslides than expected for $M7+$ earthquakes (Görüm et al., 2011). Indeed, despite the similarities of magnitude, topology, climate, and rock type, the difference between the 2015 M_w 7.8 Gorkha, Nepal, and the 2008 Wenchuan earthquake-triggered landslide densities is mainly associated with the rupture complexities (Roback et al., 2018; Xu et al., 2016). For that reason, we also investigate the effect of rupture properties of the Palu earthquake on ground motion and consequent landslide triggering in the near field.

We aim to understand whether the ground motion and the consequent landslide-triggering impact during the Palu earthquake were mitigated by the lower rupture speed or aggravated by wave amplification due to a damage zone. Among the source properties, rupture speed significantly affects ground motion: A supershear rupture can generate stronger ground motion than a subshear rupture, except if the rupture propagates at sub-Eshelby speed (Aagaard & Heaton, 2004; Bizzarri & Spudich, 2008; Dunham & Archuleta, 2005). On the other hand, waves trapped by a LVFZ can amplify ground motion (Ben-Zion et al., 2003; Huang et al., 2014; Kurzon et al., 2014; Peng et al., 2003; Spudich & Olsen, 2001). The Palu earthquake is a sub-Eshelby supershear rupture (relative to the host-rock wave speed) and may have occurred within a LVFZ: Rupture speed and fault zone structure may have had competing effects on ground motion. Therefore, the second question we address, in section 3, is: In the presence of a LVFZ, can a supershear rupture running at the damaged-rock *P* wave speed aggravate near-field ground motion?

2. Early and Sustained Supershear at Damaged-Rock *P* Wave Speed

2.1. The 2.5-D Dynamic Rupture Modeling

We model a dynamic rupture on a vertical strike-slip fault with finite seismogenic width W. For the sake of computational efficiency, we adopt a reduced-dimensionality (2.5-D) model, which has been shown to be a successful approximation of 3-D rupture models on elongated faults (Weng & Ampuero, 2019). The 2.5-D approach is derived by isolating a single vertical Fourier mode to account for the constrained depth profile of slip. This enables numerical simulations that approximately account for the 3-D effect of a finite rupture depth at the same computational cost as a 2-D simulation. The fault bisects a LVFZ with uniform properties, embedded in an unbounded, homogeneous host rock medium (Figure 1b). The LVFZ is defined by its width H and its reduction of P and S wave velocities relative to the host rock, $\Delta V/V$. We set $\Delta V/V = 30\%$, as hypothesized by Bao et al. (2019). Such a value of velocity reduction is not unusual in mature fault zones (Huang & Ampuero, 2011). We set a Poisson's ratio of 0.25 everywhere.

We artificially initiate the rupture by prescribing a smooth time-weakening front that expands at a prescribed speed, $0.25V_s$, as in Andrews (1985). The rupture starts to propagate spontaneously when the time-weakening front exceeds a critical nucleation length. Outside the time-weakening zone, the fault is controlled by the linear slip-weakening friction law (Ida, 1972; Palmer & Rice, 1973), with static and dynamic friction coefficients $\mu_s = 0.6$ and $\mu_d = 0.1$, respectively, and critical slip distance D_c. A dynamic friction of 0.1 is typical in laboratory experiments at high slip rates (Di Toro et al., 2011).

We normalize all spatial parameters by the characteristic frictional length $L_c = GD_c/\sigma(\mu_s - \mu_d)$, where G is the shear modulus and σ is the fault normal stress, which is constant during the simulation owing to the symmetries of the problem. This length is proportional to the process-zone size that must be well resolved by the numerical grid (Day et al., 2005). Due to computational constraints, we assume $L_c = 400$ m. This corresponds to a D_c value of 0.4 m, assuming $G = 30$ GPa in the host rock and a strength drop ($\sigma(\mu_s - \mu_d)$) of 30 MPa.

Huang et al. (2016) found a correlation between supershear-transition distance, normalized LVFZ width H/L_c and initial background stress. We quantify the initial background stress by the ratio $\Delta\tau_r$ of stress drop (difference between initial shear stress and dynamic shear strength $\sigma\mu_d$) to strength drop $\sigma(\mu_s - \mu_d)$. For a given $\Delta\tau_r$, the supershear-transition distance increases as a function of H/L_c. Here, we set $H = 2L_c$ to mimic the early supershear transition of the Palu earthquake for a considerably wide range of initial stress conditions. LVFZ widths most often range between 100 and 400 m, with some exceptions exceeding 1 km (e.g., Faulkner et al., 2003; Huang & Ampuero, 2011; Li & Malin, 2008; Weng et al., 2016). There is no available observation of LVFZ in Palu; we assumed a LVFZ width of 800 m to limit the computational cost. We set the seismogenic width as $W = 30L_c$, which corresponds to 12 km.

The simulations are done with the spectral element code SEM2DPACK (Ampuero, 2002, 2012). We set the element size sufficiently small to resolve the process-zone size: $0.1L_c$ and $0.5L_c$ with nine Gauss-Lobatto-Legendre nodes per element edge in the LVFZ and host-rock media, respectively. The mesh is shown in Figure S7 in the supporting information. Numerical oscillations are mitigated by artificial damping around the fault by using a viscous material of Kelvin-Voigt type (Ampuero, 2008; Galvez et al., 2014). The model domain and the duration of the simulation are chosen such that the rupture does not reach the fault end, and spurious numerical reflections at the model boundaries do not reach the rupture. Absorbing boundaries are used at all model boundaries (Clayton & Engquist, 1977).

2.2. Results

Our analyses show that, even when accounting for the finite seismogenic width, the supershear transition can occur early if the background stress is sufficiently high. We performed simulations at different background stress ratios ranging from 0.2 to 0.48. Figure 1c shows the supershear-transition distance for each case, compared to the results without W effect (2-D simulations equivalent to $W = \infty$). The transition occurs at shorter distances for a higher initial stress. This trend is qualitatively similar to that in the infinite-W case; the effect of the seismogenic depth slightly delays the supershear transition, by less than 20%. The calculated transition distance ranges roughly from 4 to 15 km if $\Delta\tau_r$ ranges from 0.3 to 0.5. Considering the uncertainties of relative location in the backprojection imaging of the Palu earthquake by Bao et al. (2019), these models are consistent with the observed early supershear-transition distance.

The observed rupture speed of the Palu event is not surprisingly low if we consider a damaged fault, as proposed by Bao et al. (2019) based on 2-D dynamic models by Huang et al. (2016): Our 2.5-D analyses confirm that the presence of a LVFZ can enable a steady-state supershear rupture at the damaged-rock P wave speed also on an elongated fault. This is well illustrated by the rupture properties in one of the cases where the supershear transition distance is consistent with the observation, namely, the case $\Delta\tau_r = 0.37$. The distribution of slip rate as a function of distance along strike and time is shown in Figure 1d. The rupture is initially subshear and transitions to supershear at a distance of 20 L_c (corresponding to 8 km). The rupture speed stabilizes at $\sim 1.2V_s$ (Figure 1e), which is the P wave speed of the LVFZ medium. Given the observed rupture speed, 4.1 km/s, for an approximate S wave speed of host rock of 3.5 km/s for the Palu event, the results of our dynamic rupture modeling support the possibility that the LVFZ presence promotes a persistent supershear rupture at damaged-rock P wave speed.

Supershear events running at a sub-Eshelby speed relative to intact rock like the Palu earthquake should not be surprising for major faults with a pronounced damage zone. Although we focused above on a single set of parameters that represents well the short supershear-transition distance and the relatively slow rupture features of the Palu event, given that we found the W effect is not dramatic, the effect of different values of fault zone width and velocity reduction can be anticipated based on the findings of comprehensive sensitivity analyses in 2-D by Huang and Ampuero (2011) and Huang et al. (2014, 2016). According to these studies, the presence of a LVFZ leads to a lower critical stress value for supershear transition than in homogeneous media, owing to dynamic stress perturbations induced by fault zone waves. Moreover, the rupture speed depends on initial stress and LVFZ properties. If the LVFZ is too narrow (e.g., $H <\sim L_c$ if $\Delta V/V = 30\%$) the wavelength of head waves inside the LVFZ is too short to induce a permanent supershear transition at any initial stress level. If the LVFZ is too wide ($H > 6L_c$ if $\Delta V/V = 30\%$) very long distances (>100 L_c) or high initial stress values ($\Delta\tau_r > 0.45$) are required to promote supershear speed. Related features are visible in the simulation results reported by Harris and Day (1997). Thus, for the case with 30% velocity reduction, the range of LVFZ widths that likely promotes a supershear rupture with an unusual speed is $1 < H/L_c < 6$. This condition implies LVFZ widths ranging from 400 m to 2.4 km for our particular choice of L_c value. Such a range involves values near and above the upper end of real LVFZ widths. A smaller L_c value allows for a supershear rupture with an unusual speed well within the usual range of natural LVFZ widths. Therefore, rupture propagation at the speed of the Palu earthquake can be expected under a considerably wide range of conditions, supporting the relatively slow supershear hypothesis of Huang et al. (2016) for past earthquakes such as the 1906 San Francisco and the 1999 M_w 7.1 Düzce earthquakes (Bouchon et al., 2001; Ben-Zion et al., 2003; Song et al., 2008). Better constraining LVFZ properties and L_c could help to test further this hypothesis.

3. Changes in Near-Field Ground Motion During a Supershear Rupture With an Unusual Speed

3.1. The 3-D Wave Propagation Modeling

To investigate the near-field ground motions during a persistent supershear rupture, we simulated steady-state ruptures in 3-D, with prescribed constant stress drop and constant rupture speed. Following the procedure of Andrews (1985) and Dunham and Bhat (2008), we force the friction coefficient to weaken linearly as a function of time inside a process zone, which propagates at prescribed speed. At the tail of the process zone, the friction coefficient equals μ_d. To avoid stress singularities at the rupture tip, the peak fault strength and process zone size are not prescribed but vary spontaneously.

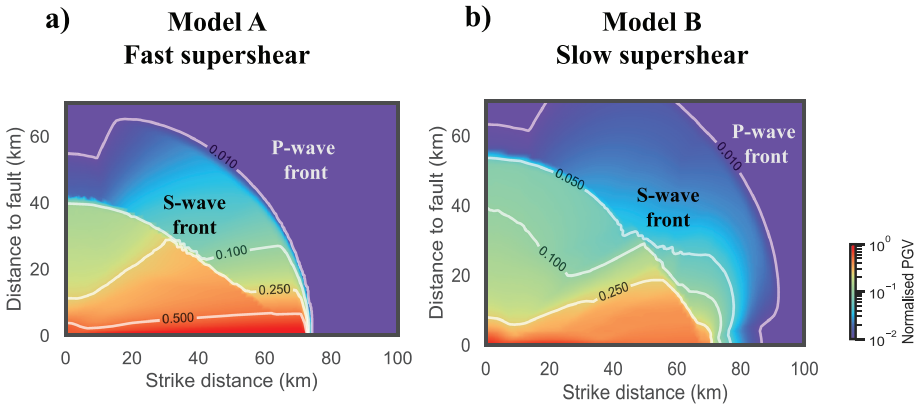

Figure 2. Maximum amplitude of the three-component ground velocity vector of (a) fast supershear and (b) slow supershear models. All values are normalized by the maximum value of Model A, which equals 5.95 m/s.

We created three different models: Model A is a fast supershear model without LVFZ; Model B is a slow supershear model with a LVFZ; and Model C is a slow supershear model without LVFZ. By "slow supershear" we mean a supershear rupture with a relatively low speed, sub-Eshelby relative to the intact rock. Model C corresponds to an artificial case because its sub-Eshelby rupture speed is inadmissible for a homogeneous host-rock medium; we use it only for comparison purposes. We set V_S = 3.5 km/s for the host rock in all models, such that V_P = 6.06 km/s, V_E = 4.95 km/s, and Poisson's ratio is 0.25. We set the rupture speed in Model A as 5.95 km/s, close to the P wave speed, and in Models B and C as 4.17 km/s, a sub-Eshelby speed. The element sizes are 0.4 and 1.2 km in the LVFZ and host-rock media, respectively. Five Gauss-Lobatto-Legendre points are used per spectral element edge. The grid allows for a resolution up to 2 Hz; we apply a Butterworth low-pass filter with 2-Hz corner frequency to all simulated signals before analysis. The model length, width, and depth are 360, 180, and 36 km, respectively. We set the seismogenic width to 12 km. Spurious numerical reflections from model boundaries are mitigated by absorbing boundary layers. We stop the simulations when the rupture has propagated a distance of 72 km (i.e., 6°W). The simulations are conducted with the SPECFEM3D software (Galvez et al., 2014; Kaneko et al., 2008; Tromp et al., 2008), which was verified in the Southern California Earthquake Center-U.S. Geological Survey dynamic rupture code verification benchmark (Harris et al., 2011, 2018). We verified that the final slip is similar in the three models (differences are of about 10%).

We evaluated the induced-landslide potential, in relative terms, by comparing seismic intensity parameters. Many studies of coseismic landslide susceptibility have used seismic intensity parameters such as peak ground velocity (PGV), peak ground acceleration, and Arias intensity (I_a). Several quantitative analyses on past coseismic landslides also point to the correlation between these parameters and observed distribution patterns of landslides (e.g., Meunier et al., 2007; Refice & Capolongo, 2002). Although the combined use of these parameters has been proposed to improve the prediction of landslide displacement (Saygılı & Rathje, 2008), a recent comparative study suggests that all parameters produce similar results (Dreyfus et al., 2013). Therefore, in this study, we discuss the landslide-triggering impact of ground motion by using PGV. Given the limitations of our simulations to low frequency (<2 Hz), we provide peak ground acceleration and I_a results only for reference in supplementary material.

3.2. Mitigation of Near-Field Landslide Hazard by Sub-Eshelby Rupture Speed

Peak ground motion is notably attenuated due to the reduction of rupture speed. We compare the PGV of Models A and B when the rupture front has propagated a distance of 72 km (Figure 2). Given its slower rupture, this occurs later in Model B than in Model A. Therefore, the P and S wave fronts in Model B have propagated a longer distance off the fault. While the results shown here can quantitatively differ at later times, our qualitative inferences remain valid. As expected, P waves attenuate with distance in both models, and large S wave amplitudes persist to long distances within Mach cones (Figure 2). The overall spatial extension of the highest PGV values is wider in Model A than in Model B given the wide expansion of the Mach cone in Model A due to its high rupture speed.

The reduction in ground-motion amplitude is related to the significant attenuation of waves in the whole frequency band due to the slow supershear. We compare the acceleration spectra between Models A and B

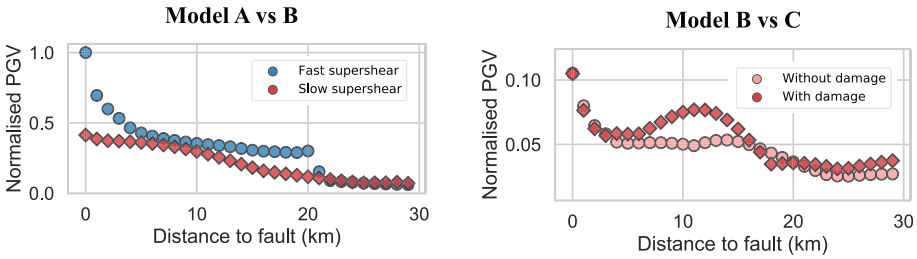

Figure 3. Comparison of peak ground velocities versus distance from the fault between fast (Model A) and slow (Model B) supershear models (a) and between slow supershear models with damage (Model B) and without damage (Model C) (b). All values are normalized by the maximum value of the Model A. The signals used in the comparison of Model B and C are high-pass filtered above 0.5 Hz to accentuate the LVFZ effect on ground motion.

at a strike distance of 40 km (Figure S1). When the rupture front reaches a distance of 72 km, the Mach cone of Model A has propagated to 22 km off the fault at 40 km along strike. Within this distance, the ground motion in Model B is weaker than in Model A at all frequencies (<2 Hz) (except for the partial amplification of low-frequency motion of Model B close to the fault in the fault-normal direction). This damping effect affects all components of ground motion at the same distance (Figure S2).

To mimic the landslide-triggering impact of our models on reported landslide locations of the Palu earthquake, we evaluate the ground motion at a fixed along-strike distance. Both submarine and inland landslides of the Palu earthquake are reported at locations that are considerably far from the fault end and where the rupture presumably propagated at a steady state. In addition, these sites are located at comparable distances in units of W, such that we interpret the landslide hazard of these sites by analyzing the ground motion at different off-fault distances but at a fixed along-strike distance.

The analyses of peak-ground velocities point to the reduction of landslide-triggering potential in the slow supershear model. We compare the dependence of PGV on off-fault distance at a strike distance of 40 km—we verified that the rupture reached steady state there—between Models A and B (Figure 3a). The largest values occur in the vicinity of the fault in both models, and the difference of PGV between the models vanishes with increasing distance to the fault. Within the distance of Mach-front propagation (<22 km), the PGV values of the fast supershear model are higher than those of the slow supershear model.

Our results support the findings of past studies: A slower rupture (here caused by the presence of a LVFZ) results in a significant reduction of the amplitudes of near-field ground motion and consequent landslide-triggering impact, and this influence of rupture speed on ground motion is valid at various distances from the fault (within 30 km here).

3.3. Enhanced High-Frequency Ground Motion and Landslide Hazard Caused by Damage

High-frequency waves are amplified due to the damaged-fault zone over a wide range of off-fault distances. To isolate the effect of the presence of a LVFZ, we compare two slow supershear models with and without a LVFZ (Models B and C, respectively). Our analysis of acceleration spectra suggests that the presence of a LVFZ results in slight amplification of the ground motion, in particular at frequencies above 0.5 Hz (Figure S4). This is expected, since the resonance frequency of waves normally reflected at the LVFZ-host rock interface is 0.39 Hz.

The high-frequency amplification due to the damaged-fault zone leads to the increase of landslide-triggering impact based on our analyses. We recall that the resolution of our model is limited to 2 Hz, and "high-frequency" here means in the frequency band of 0.5–2 Hz. Some numerical slope-stability analyses, focusing on past earthquakes that triggered massive landslides in Italy and China, report that ground motion with high energy at frequencies below 2 Hz can mobilize large volumes and be responsible for the displacement of large portions of preexisting landslide mass (Bozzano et al., 2011; Havenith et al., 2003; Martino & Mugnozza, 2005; Zhu et al., 2013). We compare the PGV values of the two models in Figure 3b. PGV decays with off-fault distance in both models, except for a certain distance range in the presence of a LVFZ in Model B; such amplification of PGV values in Model B is because of enhanced high-frequency radiation due to the LVFZ presence. To well constrain the effect of the LVFZ on PGV values, we made the comparison in the frequency band of 0.5–2 Hz; PGV amplification due to the LVFZ at a strike distance of 40 km is pronounced particularly between approximately 6 and 16 km.

The reflections due to the velocity contrast between the LVFZ and host rock can result in an amplified high-frequency motion that could also increase the landslide-triggering impact at farther distances from the fault. Considering the extent of the sites where landslides are reported (within 10-km distance from the fault), our results indicate that the landslide triggering potential of the Palu earthquake may have been aggravated by the presence of a damaged-fault zone (comparison of Models B and C). Therefore, we only focused on the amplification of ground motion in this distance range and ignored possible attenuation of ground motion at further distances. Yet, in the previous subsection, we found a dampening effect of the LVFZ on landslide triggering potential, via its effect on rupture velocity (comparison of Models A and B). Out of these two competing effects of the LVFZ, the former one (amplification) is relatively slight.

4. Conclusions and Discussion

Our 2.5-D dynamic rupture models of the Palu earthquake suggest that, for elongated-fault ruptures that saturate the seismogenic thickness, the presence of a damaged-fault zone can promote an early and persistent supershear rupture at a speed that is unexpected, namely, the *P* wave speed of the damaged rock.

The near-field ground motion produced by a supershear rupture is much weaker if it runs at the damaged-rock *P* wave speed and if this speed is lower than the Eshelby's speed of the host rock. The presence of a damaged-fault zone also amplifies high-frequency ground motion (>0.5 Hz) up to long distances from the fault (30 km). Yet the latter effect is weaker; thus, overall, the presence of a LVFZ mitigates the near-field ground motion and its landslide triggering potential.

Our findings support the strong influence of the rupture dynamics and fault zone structure on near-field ground motion and earthquake-induced landslides. The results of our simplified modeling can serve as a reference for more realistic studies where topography, heterogeneous material properties, and liquefaction potential are accounted for on a broader frequency band.

Our modeling of a damaged fault zone is limited to an elastic low-velocity zone. Understanding the effects of off-fault inelastic deformation, in the form of material plasticity and damage (Ampuero & Mao, 2017; Gabriel et al., 2013; Thomas et al., 2017; Xu et al., 2015), on rupture dynamics and ground motion deserves a further comprehensive study.

Our results can be helpful for further understanding the role of LVFZs on past and future earthquakes (e.g., Perrin et al., 2016). For example, the presence of a damaged-fault zone was speculated as an explanation of the difference of rupture speed between the northern and southern sides of the fault during the 1999 M_w 7.4 İzmit earthquake (Bouchon et al., 2001). Mai (2019) draws attention to the striking similarities between the İzmit and Palu cases for further earthquake mitigation programs—the rupture of İzmit earthquake also propagated for 150 km on a strike-slip fault, and coseismic tsunamis were triggered and locally amplified presumably because of tectonic subsidence and submarine landslides within the narrow İzmit Bay (Yalçıner et al., 2000).

Acknowledgments
This work was supported by the French National Research Agency (ANR) through project FAULTS_R_GEMS (Grant ANR-17-CE31-0008) and Investments-in-the-Future project UCAJEDI (Grant ANR-15-IDEX-01). We acknowledge Luis A. Dalguer for helpful comments that improved the content of this manuscript. All data needed to reproduce this work are available online: 2-D and 3-D wave propagation modeling tools can be found at the websites (https://github.com/jpampuero/sem2dpack and https://github.com/geodynamics/specfem3d).

References

Aagaard, B. T., & Heaton, T. H. (2004). Near-source ground motions from simulations of sustained intersonic and supersonic fault ruptures. *Bulletin of the Seismological Society of America*, *94*(6), 2064–2078.

Ampuero, J.-P. (2002). Etude physique et numérique de la nucléation des séismes (PhD Thesis), University of Paris VII, France.

Ampuero, J. P. (2008). Sem2dpack: A spectral element method tool for 2D wave propagation and earthquake source dynamics. User's guide, version 2(0).

Ampuero, J.-P. (2012). A spectral element method tool for 2D wave propagation and earthquake source dynamics user's guide.

Ampuero, J. P., & Mao, X. (2017). Upper limit on damage zone thickness controlled by seismogenic depth. *Fault Zone Dynamic Processes: Evolution of Fault Properties During Seismic Rupture*, *227*, 243.

Andrews, D. (1976). Rupture velocity of plane strain shear cracks. *Journal of Geophysical Research*, *81*(32), 5679–5687.

Andrews, D. (1985). Dynamic plane-strain shear rupture with a slip-weakening friction law calculated by a boundary integral method. *Bulletin of the Seismological Society of America*, *75*(1), 1–21.

Bao, H., Ampuero, J.-P., Meng, L., Fielding, E. J., Liang, C., Milliner, C. W., et al. (2019). Early and persistent supershear rupture of the 2018 magnitude 7.5 Palu earthquake. *Nature Geoscience*, *12*(3), 200–205.

Ben-Zion, Y., Peng, Z., Okaya, D., Seeber, L., Armbruster, J. G., Ozer, N., et al. (2003). A shallow fault-zone structure illuminated by trapped waves in the karadere–duzce branch of the North Anatolian Fault, Western Turkey. *Geophysical Journal International*, *152*(3), 699–717.

Bizzarri, A., & Spudich, P. (2008). Effects of supershear rupture speed on the high-frequency content of *S* waves investigated using spontaneous dynamic rupture models and isochrone theory. *Journal of Geophysical Research*, *113*, B05304. https://doi.org/10.1029/2007JB005146

Bouchon, M., Bouin, M.-P., Karabulut, H., Toksöz, M. N., Dietrich, M., & Rosakis, A. J. (2001). How fast is rupture during an earthquake? New insights from the 1999 Turkey earthquakes. *Geophysical Research Letters*, *28*(14), 2723–2726.

Bozzano, F., Lenti, L., Martino, S., Paciello, A., & Mugnozza, G. S. (2011). Evidences of landslide earthquake triggering due to self-excitation process. *International Journal of Earth Sciences*, *100*(4), 861–879.

Bradley, K., Mallick, R., Andikagumi, H., Hubbard, J., Meilianda, E., Switzer, A., et al. (2019). Earthquake-triggered 2018 Palu Valley landslides enabled by wet rice cultivation. *Nature Geoscience*, *12*(11), 935–939.

Carvajal, M., Araya-Cornejo, C., Sepúlveda, I., Melnick, D., & Haase, J. S. (2019). Nearly instantaneous tsunamis following the Mw 7.5 2018 Palu earthquake. *Geophysical Research Letters*, *46*, 5117–5126. https://doi.org/10.1029/2019GL082578

Clayton, R., & Engquist, B. (1977). Absorbing boundary conditions for acoustic and elastic wave equations. *Bulletin of the seismological society of America*, *67*(6), 1529–1540.

Day, S. M., Dalguer, L. A., Lapusta, N., & Liu, Y. (2005). Comparison of finite difference and boundary integral solutions to three-dimensional spontaneous rupture. *Journal of Geophysical Research*, *110*, B12307. https://doi.org/10.1029/2005JB003813

Di Toro, G., Han, R., Hirose, T., De Paola, N., Nielsen, S., Mizoguchi, K., et al. (2011). Fault lubrication during earthquakes. *Nature*, *471*(7339), 494.

Dreyfus, D., Rathje, E. M., & Jibson, R. W. (2013). The influence of different simplified sliding-block models and input parameters on regional predictions of seismic landslides triggered by the Northridge earthquake. *Engineering geology*, *163*, 41–54.

Dunham, E. M. (2007). Conditions governing the occurrence of supershear ruptures under slip-weakening friction. *Journal of Geophysical Research*, *112*, B07302. https://doi.org/10.1029/2006JB004717

Dunham, E. M., & Archuleta, R. J. (2005). Near-source ground motion from steady state dynamic rupture pulses. *Geophysical Research Letters*, *32*, L03302. https://doi.org/10.1029/2004GL021793

Dunham, E. M., & Bhat, H. S. (2008). Attenuation of radiated ground motion and stresses from three-dimensional supershear ruptures. *Journal of Geophysical Research*, *113*, B08319. https://doi.org/10.1029/2007JB005182

Faulkner, D., Lewis, A., & Rutter, E. (2003). On the internal structure and mechanics of large strike-slip fault zones: Field observations of the carboneras fault in southeastern Spain. *Tectonophysics*, *367*(3-4), 235–251.

Gabriel, A.-A., Ampuero, J.-P., Dalguer, L., & Mai, P. M. (2013). Source properties of dynamic rupture pulses with off-fault plasticity. *Journal of Geophysical Research: Solid Earth*, *118*, 4117–4126. https://doi.org/10.1002/jgrb.50213

Galvez, P., Ampuero, J.-P., Dalguer, L. A., Somala, S. N., & Nissen-Meyer, T. (2014). Dynamic earthquake rupture modelled with an unstructured 3-D spectral element method applied to the 2011 $M9$ Tohoku earthquake. *Geophysical Journal International*, *198*(2), 1222–1240.

Görüm, T., Fan, X., van Westen, C. J., Huang, R. Q., Xu, Q., Tang, C., & Wang, G. (2011). Distribution pattern of earthquake-induced landslides triggered by the 12 May 2008 Wenchuan earthquake. *Geomorphology*, *133*(3-4), 152–167.

Harris, R. A., Barall, M., Aagaard, B., Ma, S., Roten, D., Olsen, K., et al. (2018). A suite of exercises for verifying dynamic earthquake rupture codes. *Seismological Research Letters*, *89*(3), 1146–1162.

Harris, R. A., Barall, M., Andrews, D. J., Duan, B., Ma, S., Dunham, E. M., et al. (2011). Verifying a computational method for predicting extreme ground motion. *Seismological Research Letters*, *82*(5), 638–644.

Harris, R. A., & Day, S. M. (1997). Effects of a low-velocity zone on a dynamic rupture. *Bulletin of the Seismological Society of America*, *87*(5), 1267–1280.

Havenith, H.-B., Strom, A., Calvetti, F., & Jongmans, D. (2003). Seismic triggering of landslides. Part B: Simulation of dynamic failure processes. *Natural Hazards and Earth System Science*, *3*(6), 663–682.

Huang, Y., & Ampuero, J.-P. (2011). Pulse-like ruptures induced by low-velocity fault zones. *Journal of Geophysical Research*, *116*, B12307. https://doi.org/10.1029/2011JB008684

Huang, Y., Ampuero, J.-P., & Helmberger, D. V. (2014). Earthquake ruptures modulated by waves in damaged fault zones. *Journal of Geophysical Research: Solid Earth*, *119*, 3133–3154. https://doi.org/10.1002/2013JB010724

Huang, Y., Ampuero, J.-P., & Helmberger, D. V. (2016). The potential for supershear earthquakes in damaged fault zones–theory and observations. *Earth and Planetary Science Letters*, *433*, 109–115.

Ida, Y. (1972). Cohesive force across the tip of a longitudinal-shear crack and griffith's specific surface energy. *Journal of Geophysical Research*, *77*(20), 3796–3805.

Kaneko, Y., Lapusta, N., & Ampuero, J.-P. (2008). Spectral element modeling of spontaneous earthquake rupture on rate and state faults: Effect of velocity-strengthening friction at shallow depths. *Journal of Geophysical Research*, *113*, B09317. https://doi.org/10.1029/2007JB005553

Keefer, D. K. (1984). Landslides caused by earthquakes. *Geological Society of America Bulletin*, *95*(4), 406–421.

Kurzon, I., Vernon, F. L., Ben-Zion, Y., & Atkinson, G. (2014). Ground motion prediction equations in the San Jacinto Fault zone: Significant effects of rupture directivity and fault zone amplification. *Pure and Applied Geophysics*, *171*(11), 3045–3081.

Li, Y.-G., & Malin, P. E. (2008). San Andreas fault damage at SAFOD viewed with fault-guided waves. *Geophysical Research Letters*, *35*, L08304. https;//doi.org/10.1029/2007GL032924

Mai, P. M. (2019). Supershear tsunami disaster. *Nature Geoscience*, *12*(3), 150.

Martino, S., & Mugnozza, G. S. (2005). The role of the seismic trigger in the Calitri landslide (Italy): Historical reconstruction and dynamic analysis. *Soil Dynamics and Earthquake Engineering*, *25*(12), 933–950.

Meunier, P., Hovius, N., & Haines, A. J. (2007). Regional patterns of earthquake-triggered landslides and their relation to ground motion. *Geophysical Research Letters*, *34*, L20408. https;//doi.org/10.1029/2007GL031337

Palmer, A. C., & Rice, J. R. (1973). The growth of slip surfaces in the progressive failure of over-consolidated clay. *Proceedings of the Royal Society of London. A. Mathematical and Physical Sciences*, *332*(1591), 527–548.

Papadopoulos, G. A., & Plessa, A. (2000). Magnitude–distance relations for earthquake-induced landslides in greece. *Engineering Geology*, *58*(3-4), 377–386.

Peng, Z., Ben-Zion, Y., Michael, A. J., & Zhu, L. (2003). Quantitative analysis of seismic fault zone waves in the rupture zone of the 1992 Landers, California, earthquake: Evidence for a shallow trapping structure. *Geophysical Journal International*, *155*(3), 1021–1041.

Perrin, C., Manighetti, I., Ampuero, J.-P., Cappa, F., & Gaudemer, Y. (2016). Location of largest earthquake slip and fast rupture controlled by along-strike change in fault structural maturity due to fault growth. *Journal of Geophysical Research: Solid Earth*, *121*, 3666–3685. https://doi.org/10.1002/2015JB012671

Refice, A., & Capolongo, D. (2002). Probabilistic modeling of uncertainties in earthquake-induced landslide hazard assessment. *Computers & Geosciences*, *28*(6), 735–749.

Roback, K., Clark, M. K., West, A. J., Zekkos, D., Li, G., Gallen, S. F., et al. (2018). The size, distribution, and mobility of landslides caused by the 2015 $Mw7$. 8 Gorkha earthquake, Nepal. *Geomorphology*, *301*, 121–138.

Saygılı, G., & Rathje, E. M. (2008). Empirical predictive models for earthquake-induced sliding displacements of slopes. *Journal of Geotechnical and Geoenvironmental Engineering*, *134*(6), 790–803.

Socquet, A., Hollingsworth, J., Pathier, E., & Bouchon, M. (2019). Evidence of supershear during the 2018 magnitude 7.5 Palu earthquake from space geodesy. *Nature Geoscience*, *12*(3), 192.

Song, S. G., Beroza, G. C., & Segall, P. (2008). A unified source model for the 1906 San Francisco earthquake. *Bulletin of the Seismological Society of America*, *98*(2), 823–831.

Spudich, P., & Olsen, K. (2001). Fault zone amplified waves as a possible seismic hazard along the Calaveras Fault in central California. *Geophysical Research Letters*, *28*(13), 2533–2536.

Thomas, M. Y., Bhat, H. S., & Klinger, Y. (2017). Effect of brittle off-fault damage on earthquake rupture dynamics. In M. Y. Thomas, T. M. Mitchell, & H. S. Bhat (Eds.), *Fault zone dynamic processes: Evolution of fault properties during seismic rupture* (Vol. 227, pp. 255). Hoboken, New Jersey: John Wiley & Sons, Inc.

Tromp, J., Komatitsch, D., & Liu, Q. (2008). Spectral-element and adjoint methods in seismology. *Communications in Computational Physics*, *3*(1), 1–32.

Watkinson, I. M., & Hall, R. (2019). Impact of communal irrigation on the 2018 Palu earthquake-triggered landslides. *Nature Geoscience*, *12*(11), 940–945.

Weng, H., & Ampuero, J.-P. (2019). The dynamics of elongated earthquake ruptures. *Journal of Geophysical Research: Solid Earth*, *124*, 8584–8610. https://doi.org/10.1029/2019JB017684

Weng, H., Yang, H., Zhang, Z., & Chen, X. (2016). Earthquake rupture extents and coseismic slips promoted by damaged fault zones. *Journal of Geophysical Research: Solid Earth*, *121*, 4446–4457. https://doi.org/10.1002/2015JB012713

Xu, S., Ben-Zion, Y., Ampuero, J.-P., & Lyakhovsky, V. (2015). Dynamic ruptures on a frictional interface with off-fault brittle damage: Feedback mechanisms and effects on slip and near-fault motion. *Pure and Applied Geophysics*, *172*(5), 1243–1267.

Xu, C., Xu, X., Tian, Y., Shen, L., Yao, Q., Huang, X., et al. (2016). Two comparable earthquakes produced greatly different coseismic landslides: The 2015 Gorkha, Nepal and 2008 Wenchuan, China events. *Journal of Earth Science*, *27*(6), 1008–1015.

Yalçıner, A. C., Altinok, Y., Synolakis, C. E., Borrero, J., Imamura, F., Ersoy, S., et al. (2000). Tsunami waves in Izmit Bay. *Earthquake Spectra*, *16*(SUPPL. A), 55–62.

Zhu, S., Shi, Y., Lu, M., & Xie, F. (2013). Dynamic mechanisms of earthquake-triggered landslides. *Science China Earth Sciences*, *56*(10), 1769–1779.